Catalysis Science & Technology

ROYAL SOCIETY OF CHEMISTRY

PAPER

View Article Online
View Journal | View Issue

Cite this: *Catal. Sci. Technol.*, 2025, **15**, 5737

Bare La_2O_3 in non-oxidative propane dehydrogenation: *in situ* decoration of active sites for enhanced catalyst performance

Tatiana Otroshchenko,* Shanlei Han, Thanh Huyen Vuong, Vita A. Kondratenko, Jabor Rabeah, Stephan Bartling and Evgenii V. Kondratenko*

Received 20th June 2025,
Accepted 30th July 2025

DOI: 10.1039/d5cy00750j

rsc.li/catalysis

To replace toxic or expensive CrO_x- or Pt-based catalysts currently used in large-scale production of propene through non-oxidative dehydrogenation of propane, ecologically friendly and cost-effective alternatives are needed. In this context, we introduce La_2O_3 as a promising catalyst for this reaction. Our characterization and catalytic experiments as well as density functional theory calculations revealed that coordinatively unsaturated La^{3+} cations (La_{cus}) possess high activity to the cleavage of the C–H bond in propane. However, they strongly adsorb propene and hydrogen atoms formed from propane, favoring the formation of coke but hindering their recovery by H_2 desorption. La_{cus} can, however, be decorated with hydrogen species in the presence of gas-phase H_2. These new species show high activity for propane activation but low ability to adsorb propene and open a more energetically favorable pathway for H_2 formation. La_2O_3 does not obviously differ from an industrial analogue of K-CrO_x/Al_2O_3 in terms of propene selectivity up to 60% equilibrium propane conversion at 600 °C using a feed with 40 vol% C_3H_8 and 30 vol% H_2 in N_2. The effect of hydrogen on the PDH performance of La_2O_3 may inspire other researchers involved in the development of alternative catalysts, which are typically tested in the absence of hydrogen.

Introduction

The production of propene, the second most important building block in the chemical industry after ethylene, has received considerable attention in recent years.[1] This chemical is applied for the manufacture of polypropylene, acrolein, acrylonitrile, propylene oxide, acetone, and other chemicals. Despite its wide range of applications, propene is still mostly produced as a by-product of cracking processes based on crude oil. Moreover, these processes cannot longer meet the increasing demand for propene. Therefore, on-purpose propene production technologies have been developed and commercialized.[2]

Non-oxidative propane dehydrogenation to propene (PDH) is the main on-purpose technology.[3–6] CrO_x- or Pt-containing catalysts applied for this process demonstrate high activity, propene selectivity and durability. However, they suffer from the high price of Pt and the environmental issues caused by Cr(VI) compounds. Consequently, many efforts have been made to develop alternative catalysts free from such drawbacks. Generally, catalysts composed of a thermally stable support material and catalytically active metal-oxide supported species (VO_x,[7–9] ZnO_x,[10–14] CoO_x,[15–18] GaO_x,[19–21] SnO_x,[22] FeO_x (ref. 23 and 24)) are the most promising candidates. Their performance is largely determined by the structure of the supported species, which is not always easy to control and to stabilize under severe reaction conditions.

In view of the above shortcomings, we have originally introduced a novel concept for the design of bulk catalysts based on ZrO_2.[25,26] Surface defects, *i.e.*, coordinatively unsaturated zirconium cations (Zr_{cus}), were concluded to be the active sites. This concept is attracting more and more attention and has led to the development of novel bulk catalysts based on TiO_2,[27–30] Al_2O_3,[31–34] Eu_2O_3,[35] and Gd_2O_3.[35] The focus of such studies has mainly been to identify ways of increasing the concentration of surface defect sites through catalyst preparation or treatment to control catalyst activity.[26,28,36,37] It is also worth noting that such materials form a relatively new class of PDH catalysts. Thus, their potential remains unexplored.

Here we present La_2O_3 as a potential PDH catalyst whose performance is unusually changed in the presence of co-fed hydrogen compared to the metal-oxide catalysts mentioned above. Both activity and propene selectivity increase with increasing partial pressure of H_2 due to *in situ* decoration of coordinatively unsaturated La^{3+} (La_{cus}) with hydrogen species. DFT calculations predict that the decorated La_{cus} sites open a new pathway for the activation of the C–H bond in propane

Leibniz-Institut für Katalyse e.V., Albert-Einstein-Str. 29a, D-18059 Rostock, Germany. E-mail: tatiana.otroshchenko@catalysis.de, evgenii.kondratenko@catalysis.de

and the formation of gas-phase H_2, and show a lower ability to adsorb propene in comparison with their undecorated counterparts. To benchmark La_2O_3, we compared its PDH performance with that of a commercial analogue of K-CrO_x/Al_2O_3 tested in parallel under industrially relevant conditions in a broad range of propane conversion degrees.

Results and discussion

Catalytic performance in propane dehydrogenation

Hydroxycarbonates/carbonates formed from La_2O_3 under ambient conditions due to its hygroscopicity and basicity[38,39] (Fig. S1–S3) were found to negatively influence the rate of propene formation (black solid data in Fig. 1(a)). They can be practically completely decomposed (trace amounts of carbonates are still present) after sequential treatment of La_2O_3 in oxidizing and reducing atmospheres at 600 °C (Fig. S4–S6 and the corresponding discussion below them, Table S1). The treated catalyst, called as La_2O_3 oxidized-reduced, contains oxygen vacancies detected by EPR (Fig. 1(b)) and accordingly La_{cus} sites.[40–42] It showed high initial (after 5 min on stream) rate of propene formation (blue data in Fig. 1(a)) implying that the surface defects formed during the reductive treatment are crucial for catalyst activity. However, the rate of propene formation gradually decreased with increasing time on stream due to coke formation. When La_2O_3 oxidized-

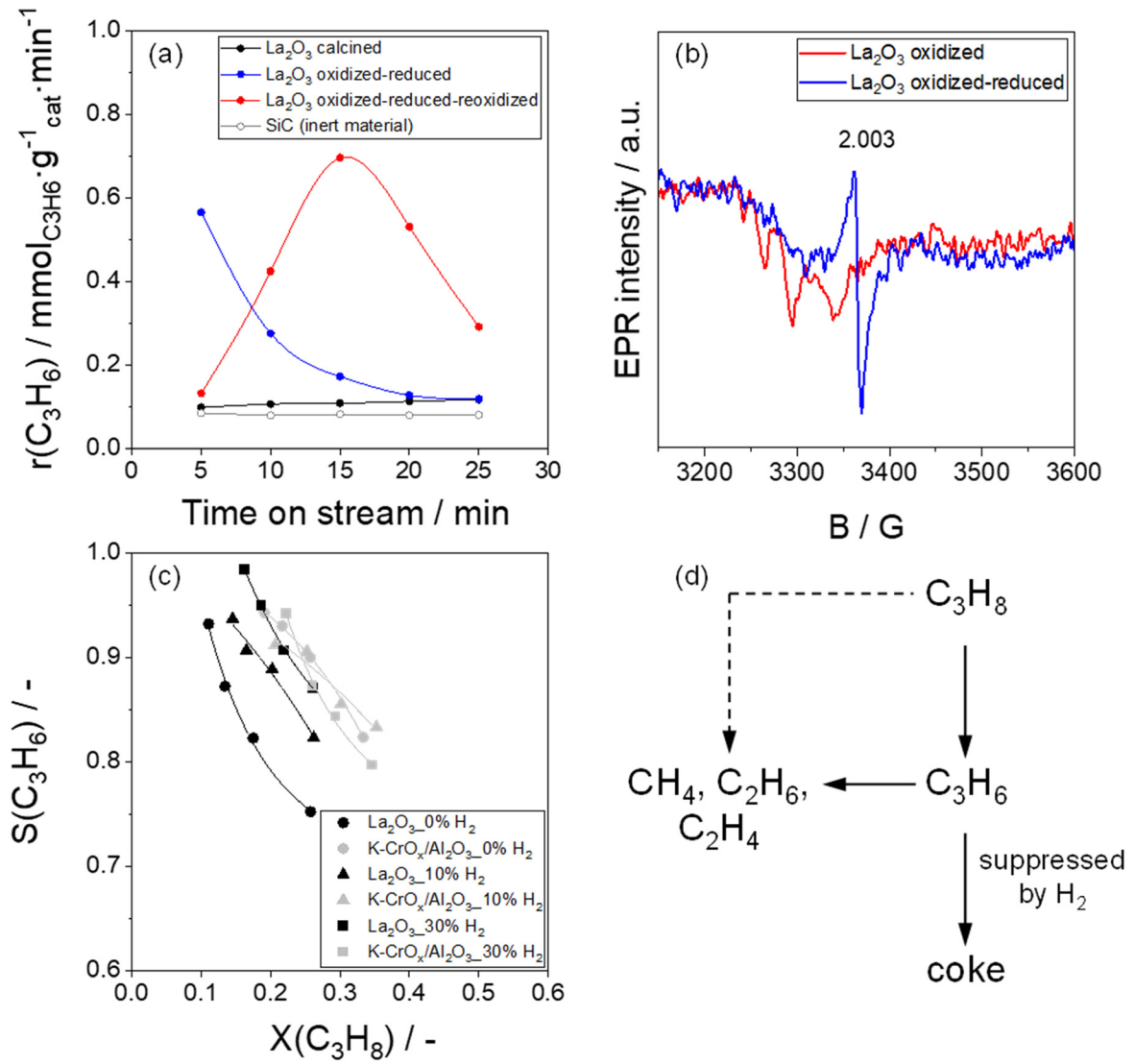

Fig. 1 (a) Temporal changes in the rate of propene formation determined at 600 °C over differently treated La_2O_3 samples. Test conditions: m_{cat} = 50 mg, 40 vol% C_3H_8 in N_2, feed flow = 20 mL min^{-1}, T = 600 °C. The rate of propene formation over inert SiC related to the gas-phase non-catalytic reaction is shown with grey color with open circles. (b) Electron paramagnetic resonance spectra of La_2O_3 after oxidative treatment (black line) and after reductive treatment followed by evacuation (red line). The spectra were recorded at −168 °C. The value of g = 2.003 is a characteristic feature of free electrons in an oxygen vacancy.[43,44] (c) Dependence of selectivity to propene on propane conversion determined for defective La_2O_3 (black symbols) and K-CrO_x/Al_2O_3 (grey symbols) using 40%C_3H_8–60%N_2 (●, ●), 40%C_3H_8–10%H_2–50%N_2 (▲, ▲), and 40%C_3H_8–30%H_2–30%N_2 (■, ■) reaction feeds at 600 °C. (d) Proposed scheme of product formation in propane dehydrogenation.

reduced was reoxidized before starting the PDH reaction, its initial activity was similar to that of the non-treated catalyst but increased with increasing time on stream and passed a maximum after 15 min. The increase should be related to the formation of La_{cus} sites *in situ*. We have also evaluated the blind (non-catalytic) activity at 600 °C, as indicated by the open symbols in Fig. 1(a). This activity is significantly lower than that of La_2O_3 samples free from hydroxycarbonates and carbonates (La_2O_3 oxidized-reduced or La_2O_3 oxidized-reduced-reoxidized in Fig. 1(a)). Therefore, we can confidently conclude that the product formation in our experiments predominantly occurs through heterogeneous catalytic pathways.

Primary and secondary reaction pathways in the course of propane dehydrogenation at 600 °C over La_2O_3 oxidized-reduced were identified by analyzing the selectivity–conversion plots of propene, C_1–C_2 hydrocarbons and carbon deposits, which were constructed based on catalytic tests carried out at different contact times (Fig. 1(c) and S7(a and b)) For comparative purposes, the corresponding relationships were determined for an analogue of the industrial K-CrO_x/Al_2O_3 catalyst. The selectivity to propene decreases with increasing propane conversion over both samples due to consecutive transformations of this olefin (Fig. 1(c)). However, the strength of the decrease is larger for La_2O_3 than for K-CrO_x/Al_2O_3. The selectivity to C_1–C_2 hydrocarbons over these catalysts increases with increasing propane conversion starting from a non-zero value (nearly 5%) at zero conversion (Fig. S7(a)) implying that these products are formed from both propane and propene. The selectivity–conversion relationships for coke differ significantly for La_2O_3 and K-CrO_x/Al_2O_3. The selectivity to coke increases with increasing propane conversion starting from zero value at zero conversion (Fig. S7(b)) and reaching values of 16% and 3% for La_2O_3 and K-CrO_x/Al_2O_3 respectively at 26% propane conversion. This dependence suggests that propene primarily formed from propane undergoes consecutive transformation to carbon deposits, with this reaction having a stronger impact on La_2O_3.

In contrast to K-CrO_x/Al_2O_3, the selectivity to propene over La_2O_3 in a broad range of propane conversions was significantly improved when the PDH reaction was performed with co-fed hydrogen (Fig. 1(c)). Noticeably, when using the reaction feed consisting of 40 vol% C_3H_8 and 30 vol% H_2 in N_2, La_2O_3 and K-CrO_x/Al_2O_3 performed very similarly in terms of selectivity to propene; 87% selectivity was achieved at 26% propane conversion over both catalysts. The increase in the selectivity to propene is due to the suppression of the formation of carbon deposits (Fig. S7(b)). The selectivity to C_1–C_2 hydrocarbons over La_2O_3 was hardly affected by co-fed hydrogen but increased over K-CrO_x/Al_2O_3 (Fig. S7(a)).

On the basis of the obtained selectivity–conversion relationships, the overall reaction pathways leading to different reaction products in the PDH reaction are similar for La_2O_3 and K-CrO_x/Al_2O_3 (Fig. 1(d)). Propene and C_1–C_2 hydrocarbons are formed from gas-phase propane as primary products. The undesired hydrocarbons are additionally formed from propene. Coke originates exclusively through consecutive transformations of propene. However, the catalysts differ in the effect of H_2 on the pathways that contribute to the loss of propene selectivity. The primary (extrapolated to zero propane conversion) selectivity to C_1–C_2 hydrocarbons over K-CrO_x/Al_2O_3 increases with increasing feed content of H_2, while a decrease was found for La_2O_3. For both catalysts, the increase in this selectivity with increasing propane conversion is not obviously affected by H_2. Based on these results, we can conclude that this reactant does not influence the propene cracking to C_1–C_2 hydrocarbons over both catalysts but positively affects the propane cracking over K-CrO_x/Al_2O_3. This reaction is partially hindered over La_2O_3. Thus, the selectivity to propene over the latter catalyst is significantly improved. Based on the hindering hydrogen effect on coke formation we assume that the desired dehydrogenation reaction and side reactions involving gas-phase propene may proceed on different sites. The unselective ones seem to competitively adsorb hydrogen and propene. It cannot be completely excluded that propene adsorbed on the unselective sites is further hydrogenated to propane. For both options, the coverage by adsorbed propene species should decrease with an increase in H_2 partial pressure resulting in hindered coke formation. It is worth mentioning that the strong positive effect of H_2 on the selectivity to propene was not previously reported for bulk ZrO_2-[45] or supported Pt-based[46] catalysts, although it is well-known that the formation of coke over Pt-based[47–49] and ZrO_2-based[45] catalysts is hindered in the presence of H_2. The H_2-mediated improvement of propene selectivity over supported GaO_x-based catalysts was ascribed to the formation of metastable gallium hydride species promoting C–H bond activation in propane but inhibiting deep dehydrogenation of propene.[50] A recent study on the H_2-mediated activity improvement of an iron-containing catalyst based on dealuminated BEA zeolite has shown that the enhancing effect is related to the increased strength of propane adsorption.[51] To provide an understanding of the effect of H_2 on the PDH reaction over La_2O_3, DFT calculations were performed. The obtained results are presented and discussed below.

Molecular-level details on propene dehydrogenation over defective La_2O_3

We firstly analyzed possible reaction pathways over the clean def-La_2O_3(001) surface in the absence of H_2. Considering the EPR results in Fig. 1(b), the constructed surface contains an anion vacancy. Different sites for dissociative propane adsorption were considered (Fig. S8). Based on the obtained energy values, we assume that the first C–H bond cleavage in adsorbed C_3H_8 proceeds with the participation of three La_{cus} cations (Fig. S8(a) and (b)). The resulting hydrogen atom is in the oxygen vacancy surrounded by these sites. The co-formed C_3H_7 intermediate is in a bridging position between two La_{cus} sites. The C–H bond cleavage on the La_{cus}–O pair (Fig. S8(d), (h) and (i)) or with the participation of non-defective La cations located far from the anion vacancy (Fig. S8(c), (f) and

(g)) is thermodynamically less favored. The energy required to form n-C_3H_7 (methyl C–H bond activation, Fig. S8(e)) is slightly lower (by 0.09 eV) than that to form iso-C_3H_7 (methylene C–H bond activation, Fig. S8(a)). The formation of n-C_3H_7 is also kinetically more favorable since the corresponding energy barrier is lower than that required for the formation of iso-C_3H_7 (0.17 eV *vs.* 0.31 eV, Fig. 2(a) *vs.* Fig. S9(a), and Fig. 2(c) *vs.* Fig. S9(c) (corresponding structures for the transition state TS1)). The abstraction of hydrogen from n-C_3H_7 or iso-C_3H_7 leads to the formation of adsorbed propene and another hydrogen atom located between two La_{cus} sites (structure "surf + $C_3H_6^*$ + 2H*" in Fig. 2(c) or S9(c)). The corresponding activation energies are equal to 0.74 eV (TS2 in Fig. 2(c) and S9(c)). The sequential recombination of two hydrogen atoms to form one H_2 molecule is endothermic by 1.91 eV (Fig. 2(a) and (c)). This step requires the highest energy to overcome along the entire reaction path. It is worth mentioning that the dissociative adsorption of gas-phase H_2, *i.e.*, the reverse reaction, is barrierless and leads to the formation of La_{cus} decorated with adsorbed hydrogen species (def-La_2O_3(001)-2H).

Based on the proposed reaction pathways, we also calculated the Gibbs free energies along the reaction coordinate in PDH over def-La_2O_3(001) at 600 °C (Fig. 2(b) and S9(b)). The thermodynamic corrections applied for this temperature led to some changes in the energy diagram compared to that obtained at 0 K. The propane adsorption became less favorable, propene desorption became more favorable, and the energy required for the recombination of hydrogen atoms over def-La_2O_3(001) decreased (Gibbs energy of 1.39 eV). Nevertheless, the latter step still requires the highest energy and therefore can be considered as the rate-limiting step. The theoretical conclusion about the rate-limiting step in PDH over defective La_2O_3 was further validated by transient experiments in the TAP reactor (Fig. S10).

Given previous DFT studies on the molecular aspects of the PDH reaction over ZrO_2 and TiO_2 with catalytically active Zr_{cus} and Ti_{cus} sites, respectively, we attempted to identify the similarities and differences between these metal oxides and La_2O_3. Fig. S11 shows the most favorable PDH pathways proposed for the defective h-La_2O_3(001) (this work), m-$ZrO_2(\bar{1}11)$,[26] and a-TiO_2(101).[28] The PDH reaction over all catalysts proceeds through a stepwise mechanism, which involves the sequential abstraction of hydrogen atoms from the propane molecule. However, the dissociation of C–H bonds proceeds on different sites depending on the kind of catalyst. Thus, the first and second hydrogen abstraction steps on the defective h-La_2O_3(001) involve the participation

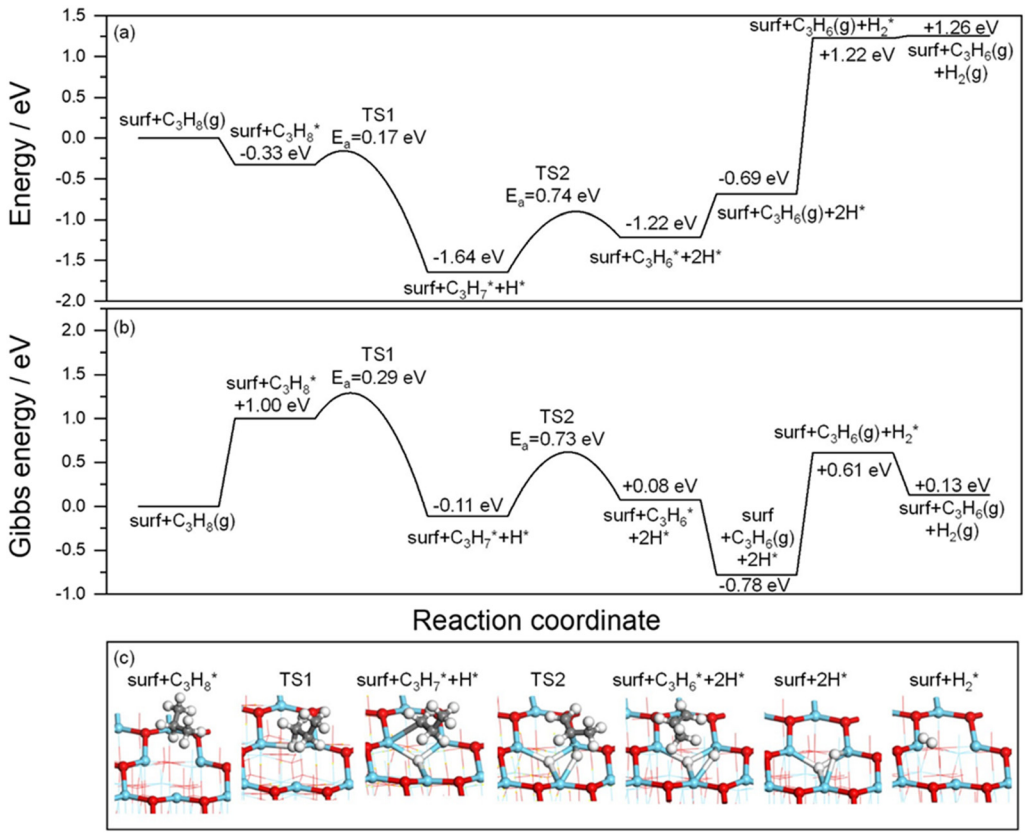

Fig. 2 The calculated (a) energy profile along the pathways of propane dehydrogenation to propene over def-La_2O_3(001) proceeding through the methyl C–H bond activation, and (b) the corresponding Gibbs free energy profile at 873 K and ambient pressure. (c) The optimized structures of intermediates and transition states. Color scheme: La – aqua, O – red, C – grey, H – white. The coordinates of the illustrated structures are provided in the section "Optimized fractional coordinates" in the SI.

of three and two La_{cus} sites respectively. Contrarily, these processes involve two and one Zr_{cus} sites on the defective m-$ZrO_2(\bar{1}11)$ surface, and the Ti_{cus}–O^{2-} pair and three Ti_{cus} sites on the defective a-$TiO_2(101)$ surface. It is however worth mentioning that for all proposed pathways, the recombination of hydrogen atoms to hydrogen molecules was identified as the rate-limiting step. Since coordinatively unsaturated cations tend to increase their saturation, they form strong bonds with hydrogen atoms introduced into the vacancy, which makes hydrogen recombination difficult. The recovery of the clean defective surface in the end of the catalytic cycle seems to be a general challenging problem of PDH catalysts based on bulk metal oxides with coordinatively unsaturated cations acting as active sites. Considering the H_2-mediated improvements in propene selectivity (Fig. 1(c and d) and 6) and inspired by the recent work on the PDH reaction over gallium hydride,[50] we analyzed if La_{cus} decorated with adsorbed hydrogen species can play a role in the PDH reaction. Such hydrogen-decorated La_{cus} sites can be formed *in situ* in the presence of hydrogen as explained below.

Hydrogen-decorated La_{cus} as active sites for propane dehydrogenation

The presence of oxygen vacancy on the surface of $La_2O_3(001)$ leads to the charge redistribution for each La atom located near this vacancy. Thus, according to Bader charge analysis, the average valence state of surface La in stoichiometric $La_2O_3(001)$ is 2.01*e* (Fig. 3(a)), while this value decreases to 1.61*e* for La_{cus} in def-$La_2O_3(001)$ (Fig. 3(b)). To compensate for the lack of surface oxygen, La_{cus} sites form very strong bonds with adsorbates. Under H_2 atmosphere, hydrogen can bond to La_{cus} sites to form def-$La_2O_3(001)$-H and def-$La_2O_3(001)$-2H. The surface energies of def-$La_2O_3(001)$, def-$La_2O_3(001)$-H, and def-$La_2O_3(001)$-2H were calculated to evaluate their relative stability at different H_2 partial pressures at 600 °C (Fig. S12). Our findings suggest that the def-$La_2O_3(001)$ surface can interact with H_2 to form def-$La_2O_3(001)$-H and def-$La_2O_3(001)$-2H at very low H_2 pressures. The introduction of hydrogen to the oxygen vacancy causes the charge compensation to the La_{cus} sites and electron redistribution with a charge accumulation over H atom(s) (Fig. 3(c)–(f)). Comparing the average Bader net atomic charge values for La on different surfaces (Fig. 3(a)–(d)), we can conclude that the concentration of electron density at La cations decreases in the following order: def-$La_2O_3(001)$ > def-$La_2O_3(001)$-H > def-$La_2O_3(001)$-2H > $La_2O_3(001)$. For the stoichiometric $La_2O_3(001)$, all surface La cations have the same valence state (2.01*e*), while for other surfaces, the La cations located near to the vacancy (empty or decorated with hydrogen) have a lower valence state than the cations located far from the vacancy. Accordingly, La cations bonded to H on def-$La_2O_3(001)$-H and def-$La_2O_3(001)$-2H surfaces are more coordinatively saturated than the La_{cus} surrounding oxygen vacancies, but still can be considered as "defect sites" since they have higher electron density than the non-defective La cations on the surface of the stoichiometric $La_2O_3(001)$.

Based on the above discussion we analyzed possible reaction pathways leading to C_3H_6 and H_2 from C_3H_8 over def-$La_2O_3(001)$-2H (Fig. 4). The latter species formed as a result of hydrogen dissociation on defective $La_2O_3(001)$ has one hydrogen atom located deep in the oxygen vacancy and another one located in the bridge position between two La_{cus} sites. While the first H atom is hardly accessible, the second H atom can interact with the H atom from the propane molecule leading to its extraction and the formation of H_2. This step has an energy barrier of 1.01 eV, which is the highest along the entire reaction path (Fig. 4(a)). After hydrogen desorption, the second hydrogen abstraction from

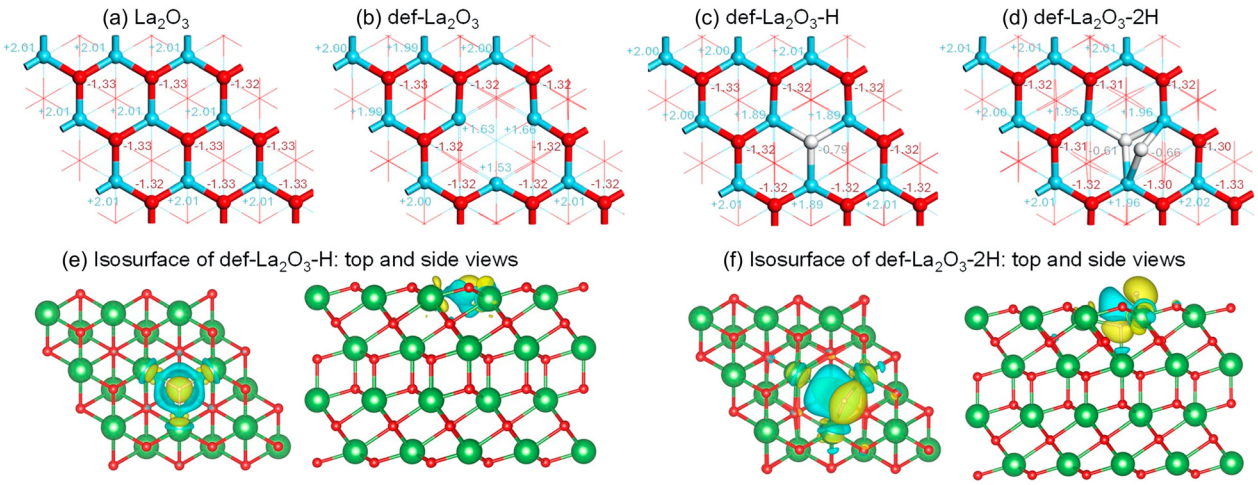

Fig. 3 The optimized structures of (a) stoichiometric $La_2O_3(001)$, (b) def-$La_2O_3(001)$, (c) def-$La_2O_3(001)$-H, and (d) def-$La_2O_3(001)$-2H with Bader net atomic charge of each element (δ = ZVAL − Bader population). Charge density difference isosurfaces (top and side views) obtained upon introduction of (e) one and (f) two H into def-$La_2O_3(001)$. Isosurface level = 0.002. The yellow and blue isosurfaces represent accumulation and depletion of electrons, respectively.

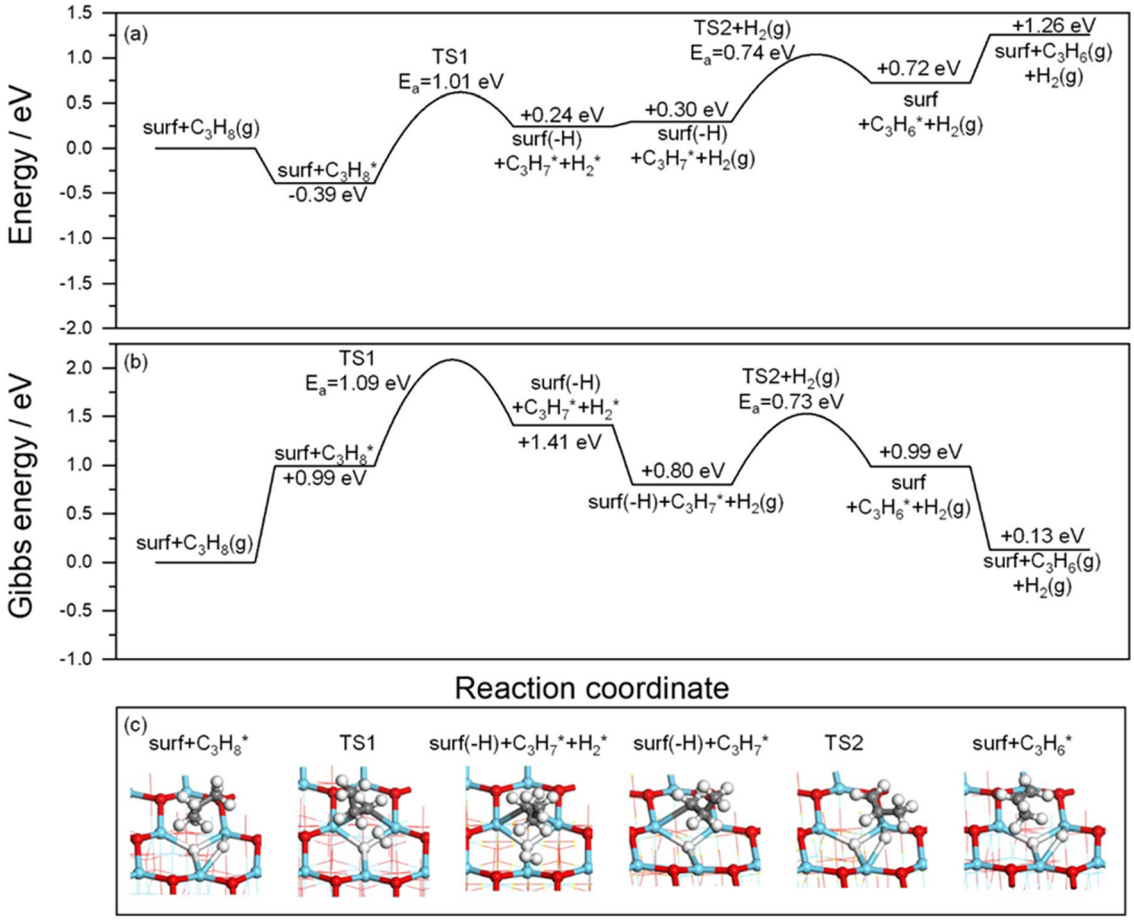

Fig. 4 The calculated (a) energy profile along the pathways of propane dehydrogenation to propene over def-La_2O_3(001)-2H proceeding through the methyl C–H bond activation and (b) the corresponding Gibbs free energy profile at 873 K and ambient pressure. (c) The optimized structures of intermediates and transition states. Color scheme: La – aqua, O – red, C – grey, H – white. The coordinates of the illustrated structures are provided in the section "Optimized fractional coordinates" in the SI.

the remaining *n*-C_3H_7 located in a bridging position between two La_{cus} sites leads to the formation of adsorbed propene and H atom, which replenishes the missing H atoms on the catalyst surface. This step has a barrier of 0.74 eV and involves the same intermediates and transition state proposed for def-La_2O_3(001). The corresponding Gibbs free energy profile was calculated based on the proposed reaction pathway (Fig. 4(b)). Since the highest energy is required for the first breakage of the C–H bond, this step can be considered as the rate-limiting one. For comparison, we schematically illustrated the propane dehydrogenation mechanism over bare def-La_2O_3(001) and def-La_2O_3(001)-2H surfaces in Fig. 5(a) and (b) respectively.

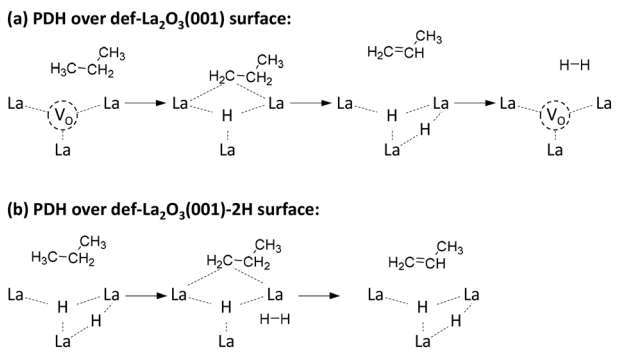

Fig. 5 Schematic illustration of the propane dehydrogenation mechanism over (a) bare def-La_2O_3(001) and (b) def-La_2O_3(001)-2H.

Coke formation and catalyst deactivation/regeneration ability

Since coke formation is the main reason for the catalyst deactivation, we also analyzed which species can be responsible for this undesired side reaction and why it is suppressed by co-fed hydrogen. According to Fig. 1(c and d) and S7(b), coke is formed through sequential reactions involving gas-phase propene, which must be adsorbed. We can assume that the higher the propene adsorption, the higher the possibility of its participation in such reactions. To analyze the strength of propene adsorption, we created models for adsorbed propene on each surface (def-La_2O_3(001), def-La_2O_3(001)-H, def-La_2O_3(001)-2H, and La_2O_3(001)) and calculated the corresponding values of energy of propene adsorption $E_{ads}(C_3H_6)$ (Fig. 6). The lowest

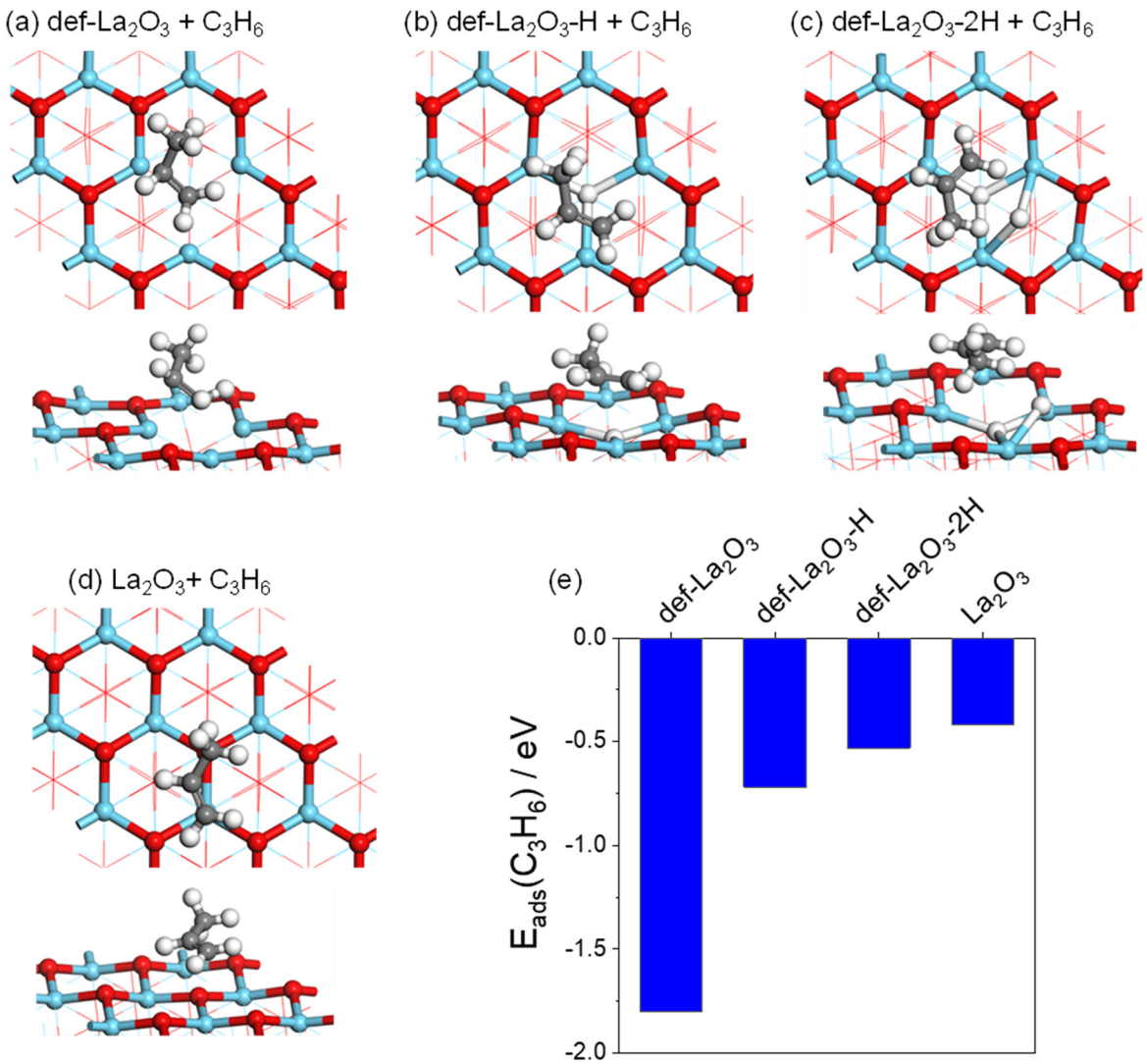

Fig. 6 The optimized structures (top and side views) of adsorbed C_3H_6 species on (a) def-La_2O_3(001), (b) def-La_2O_3(001)-H, (c) def-La_2O_3(001)-2H, and (d) La_2O_3(001). (e) The corresponding values of the energy of C_3H_6 adsorption.

$E_{ads}(C_3H_6)$ value was obtained for def-La_2O_3(001), confirming that the presence of highly unsaturated La cations significantly enhances the strength of adsorption. By decorating these sites with hydrogen, they become more saturated, and the $E_{ads}(C_3H_6)$ value becomes less negative indicating a decrease in the adsorption strength. The $E_{ads}(C_3H_6)$ value for the def-La_2O_3(001)-2H surface is very close to that of stoichiometric La_2O_3(001) (−0.53 eV *versus* −0.42 eV). Accordingly, although def-La_2O_3(001) demonstrated quite low activation energy for the first C–H bond cleavage in C_3H_8 (Fig. 2) implying high dehydrogenation ability of this surface, low coordination of active La_{cus} sites makes this surface also vulnerable to coking. On the other hand, def-La_2O_3(001)-2H is characterized by higher E_a value for the first C–H bond cleavage in C_3H_8, however it possesses increased resistance to coke formation.

Finally, we investigated the durability of defective La_2O_3 in a series of 10 PDH/regeneration cycles at 600 °C under industrially relevant conditions (propane conversion and reaction feed). Since the usage of H_2-containing feed is favorable for achieving high propene selectivity, we used the reaction mixture with 40 vol% C_3H_8 and 30 vol% H_2 in N_2. The time on stream profiles of propane conversion and propene selectivity determined in each PDH cycle are shown in Fig. S13(a) and (b) respectively. The conversion decreased with increasing time on stream within the first PDH cycle. In the second PDH cycle, the oxidized-reduced catalyst demonstrated about 20% higher initial activity, which decreased stronger with time on stream than in the first PDH cycle. The performance of the catalyst in the following PDH cycles did not change significantly from cycle to cycle. Thus, coke deposits, which were formed during PDH and led to catalyst deactivation, could be completely removed during catalyst oxidative regeneration. It is however worth mentioning that we cannot exclude some irreversible structural changes caused by high temperature since the

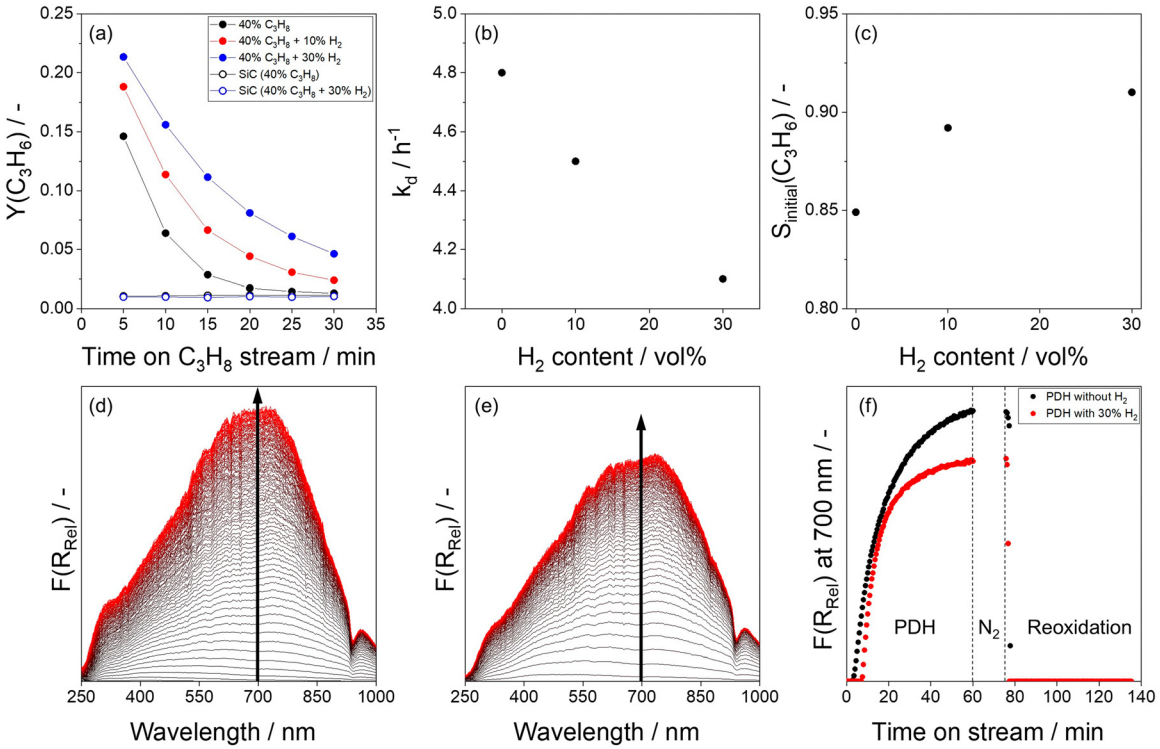

Fig. 7 (a) Temporal changes in the propene yield over La_2O_3 at 600 °C in PDH stages using feeds with 40 vol% C_3H_8 and different amounts of H_2 (0, 10, or 30 vol%) in N_2. Dependence of H_2 content in the reaction mixture on (b) the apparent deactivation constant and (c) the initial (after 5 min on C_3H_8 stream) selectivity to propene. Test conditions: m_{cat} = 300 mg, the total feed flow = 20 mL min^{-1}. UV-vis spectra ($F(R_{rel})$) of La_2O_3 after different times on PDH stream at 600 °C (d) in the absence of H_2 and (e) in the presence of 30 vol% H_2. (f) Temporal changes in $F(R_{rel})$ at 700 nm during PDH and reoxidation stages at 600 °C.

initial propane conversion slightly decreased from cycle to cycle. The selectivity to propene was about 90%. As side products, C_1–C_2 alkanes, coke, and C_2H_4 were formed.

To check if the presence of hydrogen influences catalyst on-stream stability, the catalyst used for 10 PDH/regeneration cycles was regenerated and tested using reaction feeds containing 40 vol% of C_3H_8 and different amounts of H_2 in N_2. Obviously, the catalyst showed higher stability when the reaction was performed in the presence of co-fed hydrogen (Fig. 7(a)). The apparent deactivation rate constant decreased from 4.8 to 4.1 h^{-1} with an increase in H_2 content from 0 to 30 vol%, respectively (Fig. 7(b)). This is due to the decrease in the formation of coke. The selectivity to propene increased, accordingly (Fig. 7(c)). The suppression of coke formation in the presence of co-fed H_2 was confirmed by the results of *in situ* UV-vis experiments (Fig. 7(d–f) and Note S1). Therefore, it is advantageous for the La_2O_3 catalyst to be used in PDH with co-fed hydrogen, both from selectivity and stability points of view.

Conclusions

In summary, we have demonstrated the potential of defective La_2O_3 for the non-oxidative dehydrogenation of propane to propene. Its activity is related to the presence of coordinatively unsaturated La^{3+} (La_{cus}) sites which are responsible for the sequential cleavage of two C–H bonds in propane to form propene. Like for other bulk catalysts such as defective ZrO_2 or TiO_2, the recombination of surface hydrogen atoms formed during the catalytic cycle over defective La_2O_3 requires the highest energy and can be defined as the rate-limiting step. Although La_{cus} sites are highly reactive for the cleavage of C–H bond, they suffer from severe deactivation due to the coke formed through the sequential reaction from propene. *In situ* decoration of La_{cus} sites with hydrogen can regulate charge density of these sites decreasing the energy of adsorption of propene and thus improving the resistance of the catalyst to coke formation. Moreover, the hydrogen-decorated La_{cus} sites open another reaction path for propane dehydrogenation differing from that proposed for bare La_{cus} sites. Owing to the strong positive effect of co-fed hydrogen, the formation of coke over La_2O_3 could be reduced and the selectivity to propene reached the level of K-CrO_x/Al_2O_3 at about 60% equilibrium conversion.

Author contributions

Conceptualization: T. O. and E. V. K.; investigation: T. O., S. H., T.-H. V., V. A. K, and S. B.; formal analysis: T. O.; visualization: T. O.; writing – original draft: T. O. All authors discussed the results and gave their approval of the final version.

Conflicts of interest

There are no conflicts to declare.

Data availability

Supplementary information is available: SI includes details for the catalyst preparation, characterization, and testing, computational details, supplementary figures, table, and note, optimized fractional coordinates. See DOI: **https://doi.org/10.1039/D5CY00750J**.

The data supporting this article have been included as part of the SI.

Acknowledgements

The authors thank Dr. Elizaveta A. Fedorova for the XRD analysis, Dr. Dmitry Sharapa for the help with DFT calculations, and Saint-Gobain NorPro for providing Al_2O_3 support material.

Notes and references

1 T. K. Phung, T. L. M. Pham, K. B. Vu and G. Busca, *J. Environ. Chem. Eng.*, 2021, **9**, 105673.
2 D. Xiang, P. Li and X. Yuan, *J. Cleaner Prod.*, 2022, **367**, 133024.
3 T. Otroshchenko, G. Jiang, V. A. Kondratenko, U. Rodemerck and E. V. Kondratenko, *Chem. Soc. Rev.*, 2021, **50**, 473–527.
4 X. Li, C. Pei and J. Gong, *Chem*, 2021, **7**, 1755–1801.
5 S. Chen, X. Chang, G. Sun, T. Zhang, Y. Xu, Y. Wang, C. Pei and J. Gong, *Chem. Soc. Rev.*, 2021, **50**, 3315–3354.
6 J. J. H. B. Sattler, J. Ruiz-Martinez, E. Santillan-Jimenez and B. M. Weckhuysen, *Chem. Rev.*, 2014, **114**, 10613–10653.
7 Y. Xie, R. Luo, G. Sun, S. Chen, Z.-J. Zhao, R. Mu and J. Gong, *Chem. Sci.*, 2020, **11**, 3845–3851.
8 C. Chen, M. Sun, Z. Hu, Y. Liu, S. Zhang and Z.-Y. Yuan, *Chin. J. Catal.*, 2020, **41**, 276–285.
9 Q.-Q. Yang, P. Hu, N.-Y. Xiu, W.-Z. Lang and Y.-J. Guo, *ChemistrySelect*, 2018, **3**, 10049–10055.
10 S. Han, D. Zhao, H. Lund, N. Rockstroh, S. Bartling, D. E. Doronkin, J.-D. Grunwaldt, M. Gao, G. Jiang and E. V. Kondratenko, *Catal. Sci. Technol.*, 2020, **10**, 7046–7055.
11 C. Chen, Z.-P. Hu, J.-T. Ren, S. Zhang, Z. Wang and Z.-Y. Yuan, *Mol. Catal.*, 2019, **476**, 110508.
12 J. Camacho-Bunquin, P. Aich, M. Ferrandon, A. B. Getsoian, U. Das, F. Dogan, L. A. Curtiss, J. T. Miller, C. L. Marshall, A. S. Hock and P. C. Stair, *J. Catal.*, 2017, **345**, 170–182.
13 D. Zhao, K. Guo, S. Han, D. E. Doronkin, H. Lund, J. Li, J.-D. Grunwaldt, Z. Zhao, C. Xu, G. Jiang and E. V. Kondratenko, *ACS Catal.*, 2022, **12**, 4608–4617.
14 D. Zhao, X. Tian, D. E. Doronkin, S. Han, V. A. Kondratenko, J.-D. Grunwaldt, A. Perechodjuk, T. H. Vuong, J. Rabeah, R. Eckelt, U. Rodemerck, D. Linke, G. Jiang, H. Jiao and E. V. Kondratenko, *Nature*, 2021, **599**, 234–238.
15 C.-W. Zhang, J. Wen, L. Wang, X.-G. Wang and L. Shi, *New J. Chem.*, 2020, **44**, 7450–7459.
16 Y. Dai, J. Gu, S. Tian, Y. Wu, J. Chen, F. Li, Y. Du, L. Peng, W. Ding and Y. Yang, *J. Catal.*, 2020, **381**, 482–492.
17 C. Chen, S. Zhang, Z. Wang and Z.-Y. Yuan, *J. Catal.*, 2020, **383**, 77–87.
18 B. Hu, A. B. Getsoian, N. M. Schweitzer, U. Das, H. Kim, J. Nildas, O. Poluektov, L. A. Curtiss, P. C. Stair, J. T. Miller and A. S. Hock, *J. Catal.*, 2015, **322**, 24–37.
19 M. W. Schreiber, C. P. Plaisance, M. Baumgärtl, K. Reuter, A. Jentys, R. Bermejo-Deval and J. A. Lercher, *J. Am. Chem. Soc.*, 2018, **140**, 4849–4859.
20 C.-T. Shao, W.-Z. Lang, X. Yan and Y.-J. Guo, *RSC Adv.*, 2017, **7**, 4710–4723.
21 K. Searles, G. Siddiqi, O. V. Safonova and C. Copéret, *Chem. Sci.*, 2017, **8**, 2661–2666.
22 H. Wang, H. Huang, K. Bashir and C. Li, *Appl. Catal., A*, 2020, **590**, 117291.
23 L. Sharma, S. C. Purdy, K. Page, S. Rangarajan, H. Pham, A. Datye and J. Baltrusaitis, *ACS Appl. Nano Mater.*, 2021, **4**, 10055–10067.
24 B. Hu, N. M. Schweitzer, G. Zhang, S. J. Kraft, D. J. Childers, M. P. Lanci, J. T. Miller and A. S. Hock, *ACS Catal.*, 2015, **5**, 3494–3503.
25 T. Otroshchenko, S. Sokolov, M. Stoyanova, V. A. Kondratenko, U. Rodemerck, D. Linke and E. V. Kondratenko, *Angew. Chem., Int. Ed.*, 2015, **54**, 15880–15883.
26 Y. Zhang, Y. Zhao, T. Otroshchenko, H. Lund, M.-M. Pohl, U. Rodemerck, D. Linke, H. Jiao, G. Jiang and E. V. Kondratenko, *Nat. Commun.*, 2018, **9**, 3794.
27 L. Q. Xiao, Z. A. Xie, S. J. Song, Z. P. Zhao, M. Ke, W. Y. Song, Z. Zhao and J. Liu, *Ind. Eng. Chem. Res.*, 2021, **60**, 1200–1209.
28 Z. Xie, T. Yu, W. Song, J. Li, Z. Zhao, B. Liu, Z. Gao and D. Li, *ACS Catal.*, 2020, **10**, 14678–14693.
29 C. F. Li, X. J. Guo, Q. H. Shang, X. Yan, C. L. Ren, W. Z. Lang and Y. J. Guo, *Ind. Eng. Chem. Res.*, 2020, **59**, 4377–4387.
30 S. Chen, Y. Xu, X. Chang, Y. Pan, G. Sun, X. Wang, D. Fu, C. Pei, Z.-J. Zhao, D. Su and J. Gong, *Science*, 2024, **385**, 295–300.
31 L. Sharma, X. Jiang, Z. L. Wu, J. Baltrus, S. Rangarajan and J. Baltrusaitis, *J. Catal.*, 2021, **394**, 142–156.
32 P. Wang, Z. Xu, T. Wang, Y. Yue, X. Bao and H. Zhu, *Catal. Sci. Technol.*, 2020, **10**, 3537–3541.
33 D. Zhao, H. Lund, U. Rodemerck, D. Linke, G. Jiang and E. V. Kondratenko, *Catal. Sci. Technol.*, 2021, **11**, 1386–1394.
34 M. Dixit, P. Kostetskyy and G. Mpourmpakis, *ACS Catal.*, 2018, **8**, 11570–11578.
35 A. Perechodjuk, V. A. Kondratenko, H. Lund, N. Rockstroh and E. V. Kondratenko, *Chem. Commun.*, 2020, **56**, 13021–13024.
36 T. Otroshchenko, O. Bulavchenko, H. V. Thanh, J. Rabeah, U. Bentrup, A. Matvienko, U. Rodemerck, B. Paul, R. Kraehnert, D. Linke and E. V. Kondratenko, *Appl. Catal., A*, 2019, **585**, 117189.
37 Y. Zhang, Y. Zhao, T. Otroshchenko, S. Han, H. Lund, U. Rodemerck, D. Linke, H. Jiao, G. Jiang and E. V. Kondratenko, *J. Catal.*, 2019, **371**, 313–324.
38 E. Muhumuza, P. Wu, T. Nan, L. Zhao, P. Bai, S. Mintova and Z. Yan, *Ind. Eng. Chem. Res.*, 2020, **59**, 21322–21332.

39 S. Bernal, F. J. Botana, R. García and J. M. Rodríguez-Izquierdo, *Thermochim. Acta*, 1983, **66**, 139–145.
40 J. X. Wang and J. H. Lunsford, *J. Phys. Chem.*, 1986, **90**, 3890–3891.
41 S. R. Sanivarapu, J. B. Lawrence and G. Sreedhar, *ACS Omega*, 2018, **3**, 6267–6278.
42 C. Gionco, M. C. Paganini, E. Giamello, R. Burgess, C. Di Valentin and G. Pacchioni, *Chem. Mater.*, 2013, **25**, 2243–2253.
43 S. Wright and R. C. Barklie, *J. Appl. Phys.*, 2009, **106**, 103917.
44 Q. Zhao, X. Wang and T. Cai, *Appl. Surf. Sci.*, 2004, **225**, 7–13.
45 T. Otroshchenko and E. V. Kondratenko, *Catal. Commun.*, 2020, **144**, 106068.
46 S. Saerens, M. K. Sabbe, V. V. Galvita, E. A. Redekop, M.-F. Reyniers and G. B. Marin, *ACS Catal.*, 2017, **7**, 7495–7508.
47 K. J. Caspary, H. Gehrke, M. Heinritz-Adrian and M. Schwefer, in *Handbook of Heterogeneous Catalysis*, Wiley-VCH Verlag GmbH & Co, KGaA, 2008.
48 S. B. Kogan, H. Schramm and M. Herskowitz, *Appl. Catal., A*, 2001, **208**, 185–191.
49 J. J. H. B. Sattler, A. M. Beale and B. M. Weckhuysen, *Phys. Chem. Chem. Phys.*, 2013, **15**, 12095–12103.
50 G. Sun, Z.-J. Zhao, L. Li, C. Pei, X. Chang, S. Chen, T. Zhang, K. Tian, S. Sun, L. Zheng and J. Gong, *Nat. Chem.*, 2024, **16**, 575–583.
51 A. Alghannam and A. T. Bell, *J. Am. Chem. Soc.*, 2025, **147**, 1677–1693.